AIP | APL Materials

Intrinsic magnetic properties of hexagonal LuFeO3 and the effects of nonstoichiometry

Jarrett A. Moyer, Rajiv Misra, Julia A. Mundy, Charles M. Brooks, John T. Heron, David A. Muller, Darrell G. Schlom, and Peter Schiffer

Citation: APL Mater. **2**, 012106 (2014); doi: 10.1063/1.4861795
View online: http://dx.doi.org/10.1063/1.4861795
View Table of Contents: http://scitation.aip.org/content/aip/journal/aplmater/2/1?ver=pdfcov
Published by the AIP Publishing

APL MATERIALS **2**, 012106 (2014)

Intrinsic magnetic properties of hexagonal $LuFeO_3$ and the effects of nonstoichiometry

Jarrett A. Moyer,[1,a] Rajiv Misra,[2] Julia A. Mundy,[3] Charles M. Brooks,[4] John T. Heron,[4] David A. Muller,[3,5] Darrell G. Schlom,[4,5,a] and Peter Schiffer[1]

[1]*Department of Physics and Frederick Seitz Materials Research Laboratory, University of Illinois at Urbana-Champaign, Urbana, Illinois 61801, USA*
[2]*Department of Physics, Pennsylvania State University, University Park, Pennsylvania 16802, USA*
[3]*School of Applied and Engineering Physics, Cornell University, Ithaca, New York 14853, USA*
[4]*Department of Materials Science and Engineering, Cornell University, Ithaca, New York 14853, USA*
[5]*Kavli Institute at Cornell for Nanoscale Science, Ithaca, New York 14853, USA*

(Received 4 November 2013; accepted 26 December 2013; published online 21 January 2014)

We used oxide molecular-beam epitaxy in a composition-spread geometry to deposit hexagonal $LuFeO_3$ (h-$LuFeO_3$) thin films with a monotonic variation in the Lu/Fe cation ratio, creating a mosaic of samples that ranged from iron rich to lutetium rich. We characterized the effects of composition variation with x-ray diffraction, atomic force microscopy, scanning transmission electron microscopy, and superconducting quantum interference device magnetometry. After identifying growth conditions leading to stoichiometric film growth, an additional sample was grown with a rotating sample stage. From this stoichiometric sample, we determined stoichiometric h-$LuFeO_3$ to have a $T_N = 147$ K and $M_s = 0.018$ μ_B/Fe. [http://dx.doi.org/10.1063/1.4861795]

Multiferroic materials are an exciting class of materials due to the potential that their ferroic order parameters (i.e., ferroelasticity, ferroelectricity, ferromagnetism) may be strongly coupled.[1,2] A material with coupling between the ferroelectric and ferromagnetic order parameters, called magnetoelectric coupling, could enable significant advancements of electric field controlled magnetic memories,[3,4] magnetic field sensors,[5,6] and tunable microwave filters.[7,8] Single phase materials that are simultaneously ferroelectric and ferromagnetic are, however, exceedingly rare due to the competing mechanisms that often drive ferroelectricity (d^0 insulators) and ferromagnetism (non-d^0 conductors).[9] This competition often leads to insulating multiferroics that are simultaneously ferroelectric and antiferromagnetic. Popular transition-metal oxide multiferroics include $BiFeO_3$[10,11] and the hexagonal rare-earth manganites, exemplified by $YMnO_3$.[12–14] In addition to commonly possessing antiferromagnetic order, multiferroics are typically relegated to low temperatures,[1,9] as in $YMnO_3$ with a Néel temperature (T_N) of 70 K, or are predicted to be unable to reverse a canted magnetization with a change in polarization, as in $BiFeO_3$,[15,16] both of which are conditions that are undesirable for technological applications.

The hexagonal rare-earth ferrites have also garnered attention as potential multiferroics. This class of materials is highlighted by $LuFe_2O_4$, which is reported to be simultaneously an improper ferroelectric and a ferrimagnet with a high T_C of 250 K;[17] its ferroelectricity has, however, lately

[a]Authors to whom correspondence should be addressed. Electronic addresses: moyerja@illinois.edu and schlom@cornell.edu

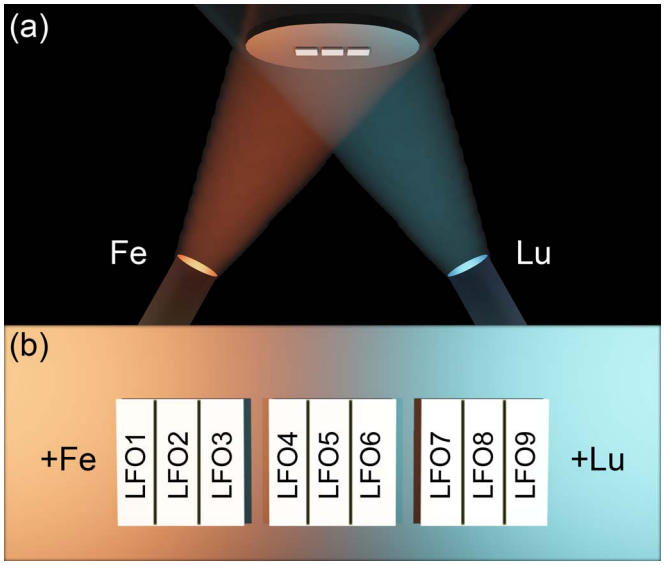

FIG. 1. (a) Schematic of composition-spread sample growth with respect to iron and lutetium effusion cells. (b) Labels for the nine composition-spread *h*-$LuFeO_3$ samples after each substrate was cut into thirds.

been called into question.[18–20] Hexagonal $LuFeO_3$ (*h*-$LuFeO_3$) is another phase in the lutetium-iron-oxygen system that has multiferroic potential. As a bulk material, $LuFeO_3$ is orthorhombic with the perovskite crystal structure, antiferromagnetic, and not ferroelectric. Using epitaxial stabilization, however, it is possible to make a metastable hexagonal polymorph of $LuFeO_3$ that is isostructural with $YMnO_3$ and other hexagonal rare-earth manganites.[21] In this hexagonal structure, $LuFeO_3$ has been measured to be both ferroelectric[22,23] and weakly ferromagnetic,[22–24] with first principles calculations predicting the ability to reverse the magnetization with a change in polarization.[25] It was recently reported that *h*-$LuFeO_3$ is antiferromagnetically ordered at room temperature with a canted antiferromagnetic ordering at $T_N = 130$ K,[23] making it one of the few known room-temperature multiferroics (in this work we will refer to the onset of canted antiferromagnetic order, which is what we can measure, as the Néel temperature).[10,11,23,26,27]

In this letter, we determine the intrinsic magnetic properties of *h*-$LuFeO_3$ by first growing a set of samples in a compositional-spread geometry that have a range of $\sim \pm 10\%$ variations in cation stoichiometry. While these films appear from x-ray diffraction (XRD) to be single phase, the nonstoichiometry becomes apparent in scanning transmission electron microscopy (STEM) and atomic force microscopy (AFM) measurements. Excess iron, which is incorporated into the film as $LuFe_2O_4$ and Fe_3O_4 impurity phases, introduces additional magnetic phases to the films, whereas excess lutetium, which does not lead to second-phase precipitates, results in a decrease in the Néel temperature of the *h*-$LuFeO_3$ phase. The combined use of microscopy and magnetometry techniques on the same composition-spread sample set enables us to identify the defects in iron-rich and lutetium-rich *h*-$LuFeO_3$ samples and correlate them with specific magnetic signatures. We then grow an additional sample, using the conditions found to yield single-phase *h*-$LuFeO_3$ obtained from the composition-spread growth, along with a rotating sample stage, to produce a nearly stoichiometric *h*-$LuFeO_3$ sample. From this sample, we establish the intrinsic magnetic properties of *h*-$LuFeO_3$.

We grew ~200 nm thick *h*-$LuFeO_3$ films by oxide molecular-beam epitaxy (MBE) in a Veeco GEN10 MBE system at a growth temperature of ~800 °C as measured by optical pyrometry. Effusion cells were used to thermally evaporate lutetium and iron at elemental fluxes of $\sim 1 \times 10^{13}$ atoms/(cm^2 s) onto 10 mm × 10 mm (111)-oriented yttria-stabilized cubic zirconia (YSZ) substrates. Oxidation of the incident lutetium and iron fluxes was provided by a mixture of oxygen and ~10% ozone supplied at a background partial pressure of 1×10^{-6} Torr. We initially aligned three YSZ substrates in a row, did *not* rotate them during growth, and deposited on them simultaneously, with the lutetium and iron effusion cells located at the opposite ends of the line of substrates [Fig. 1(a)].

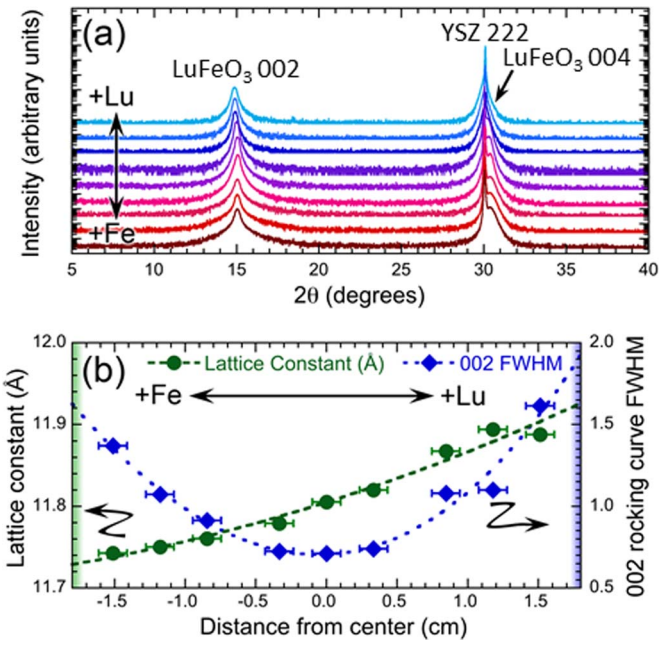

FIG. 2. (a) XRD θ-2θ scans around the 002 and 004 h-$LuFeO_3$ peaks. (b) Variation in the h-$LuFeO_3$ c-axis lattice constant and the FWHM of the rocking curve of the 002 h-$LuFeO_3$ peak with changing composition. Lines are added as a guide to the eye.

This composition-spread geometry resulted in samples with monotonically varying Lu/Fe cation ratios. We cut each substrate into thirds to create nine h-$LuFeO_3$ samples (labeled LFO1 – LFO9) that had a range of cation stoichiometries varying from iron rich to lutetium rich [Fig. 1(b)]. After ascertaining the growth conditions from the composition-spread growth that yielded single-phase h-$LuFeO_3$, we grew a nearly stoichiometric film while rotating the sample to provide homogenous cation composition throughout the entire sample. High-resolution XRD, using a four-circle Rigaku diffractometer equipped with a Ge(220)x2 monochromator on the incident side and a Ge(220)x2 analyzer on the diffracted side, with Cu K_α radiation was used to assess the structural perfection of the films. The microstructure of the samples was investigated by high-angle annular dark field scanning transmission electron microscopy (HAADF-STEM), while AFM was employed to measure the surface roughness. The magnetic properties were determined using a superconducting quantum interference device (SQUID) magnetometer (Quantum Design MPMS-XL and MPMS3).

The θ-2θ XRD scans of the composition-spread samples, displayed in Fig. 2(a), contain only the expected 00$2\underline{\ell}$ peaks and are free of impurity peaks. This implies that the films are (001) oriented and appear to be single phase. The out-of-plane (c-axis) spacing was determined using a Nelson-Riley fit[28] to the positions of the 002 and 006 h-$LuFeO_3$ film peaks. The c-axis lattice parameters of these nine samples are plotted in Fig. 2(b), which shows a systematic increase in the c-axis lattice parameter as the samples vary from iron rich to lutetium rich. Overlaid on the c-axis lattice parameters in Fig. 2(b) are the full width at half maximum (FWHM) of the rocking curve widths (in ω) for each sample. The rocking curve FWHM is near a minimum for LFO6, the sample that is nearest to stoichiometry as determined from STEM, and increases for both lutetium- and iron-rich samples. From the XRD data, it appears that each sample is single phase and highly crystalline; upon examination of the entire set of samples, however, small changes in the crystalline properties emerge that elucidate the adverse effects of nonstoichiometry on crystalline quality.

STEM images on the same samples reveal the microstructure of the h-$LuFeO_3$ films and demonstrate that not all of the samples are single phase. Figure 3 shows representative STEM images of an iron-rich sample (LFO2), a near-stoichiometric sample (LFO6), and a lutetium-rich sample (LFO8). The near-stoichiometric sample appears well ordered throughout the entire thickness of the film and contains less than one monolayer (ML) of excess iron. Due to the similar in-plane lattice

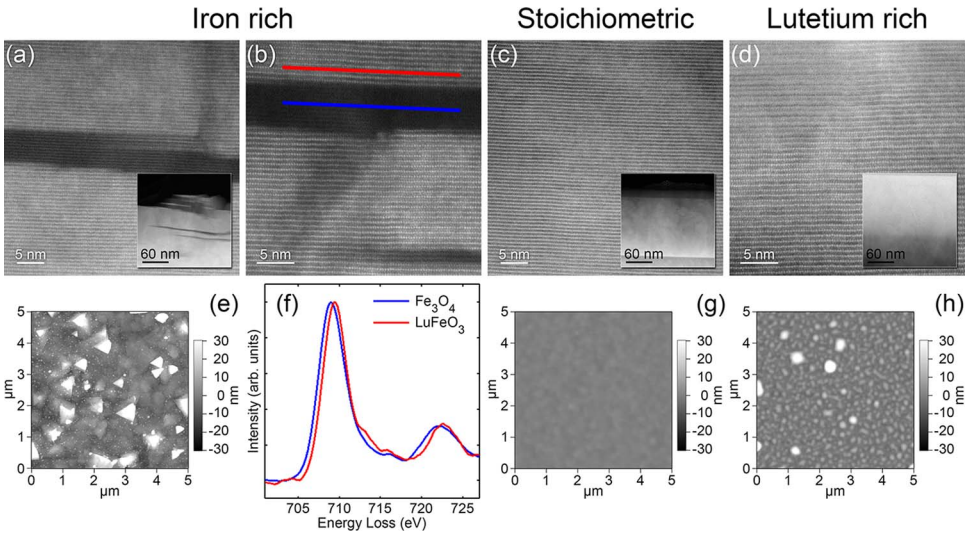

FIG. 3. STEM and AFM images for [(a) and (e)] iron-rich, [(c) and (g)] stoichiometric, and [(d) and (h)] lutetium-rich h-$LuFeO_3$ samples, respectively. The insets in the STEM images display the entire thickness of the sample. (b) STEM image of a Fe_3O_4 planar impurity phase in the h-$LuFeO_3$ matrix. (f) EELS spectra of the Fe-$L_{2,3}$ edge from the regions marked in (b).

parameters of h-$LuFeO_3$ and $LuFe_2O_4$, excess iron is easily incorporated as syntactic intergrowths of additional FeO planes, essentially creating $LuFe_2O_4$ intergrowths. Films that are iron rich, such as LFO2, can incorporate excess iron in multiple ways. Near the YSZ/h-$LuFeO_3$ interface, excess iron is incorporated as double iron oxide layers, creating $LuFe_2O_4$ intergrowths in the sample. As the sample grows thicker, excess iron is also seen incorporated as Fe_3O_4 layers that are multiple unit cells thick. We used electron energy loss spectroscopy (EELS) in the STEM to access the oxidation state of the iron in both the h-$LuFeO_3$ film and the Fe_3O_4 precipitates. Figure 3(b) shows a Fe_3O_4 precipitate within a h-$LuFeO_3$ film, and Fig. 3(f) displays their corresponding EELS spectra. The EELS spectrum of the h-$LuFeO_3$ film is consistent with that of Fe^{3+} cations. The Fe_3O_4 impurity phase exhibits a valence below that in the h-$LuFeO_3$ and is determined to be 2.68 ± 0.03,[29] near the nominal $+2.67$ oxidation state of Fe_3O_4. Previous work has reported that layers of (111)-oriented Fe_3O_4 can be epitaxially stabilized within h-$LuFeO_3$ thin films.[30] Excess lutetium, as in LFO8, does not order and is not easily detected in the STEM images. AFM scans of these samples (Fig. 3) reveal that as the samples become more nonstoichiometric, i.e., iron or lutetium rich, islands begin to appear on the surface. The islands on the lutetium-rich samples are round and likely amorphous, while the islands on the iron-rich samples are faceted and crystalline. The defects that result from nonstoichiometry, which are not readily apparent from XRD measurements, clearly distinguish themselves upon examination of the film microstructure with microscopy techniques, allowing the stoichiometric region to be distinguished within the composition spread sample.

We determined the magnetic properties of the h-$LuFeO_3$ samples by measuring the magnetic response of each sample with a SQUID magnetometer. Magnetization vs. temperature (M-T) curves, measured in a magnetic field of 100 Oe after cooling in either zero field (ZFC) or a 1 kOe field (FC), identified the different magnetic phases within each sample. Measurements of a bare YSZ substrate allowed for the diamagnetic and paramagnetic backgrounds to be subtracted. A representative out-of-plane ZFC and FC M-T curve for the near-stoichiometric sample, LFO6, is shown in Fig. 4(a). A dominant canted antiferromagnetic phase, corresponding to h-$LuFeO_3$, is clearly evident and has a $T_N \sim 141$ K; T_N was determined by extrapolating the point of steepest slope on the M-T curve to the background of the additional magnetic phases. Two smaller, high-temperature magnetic phases are also present in this measurement, which become clearer as the iron content is increased.

Figure 4(b) displays the out-of-plane FC data of the nine compositionally spread samples; as the iron content is increased, the magnetizations of the two high temperature phases both increase.

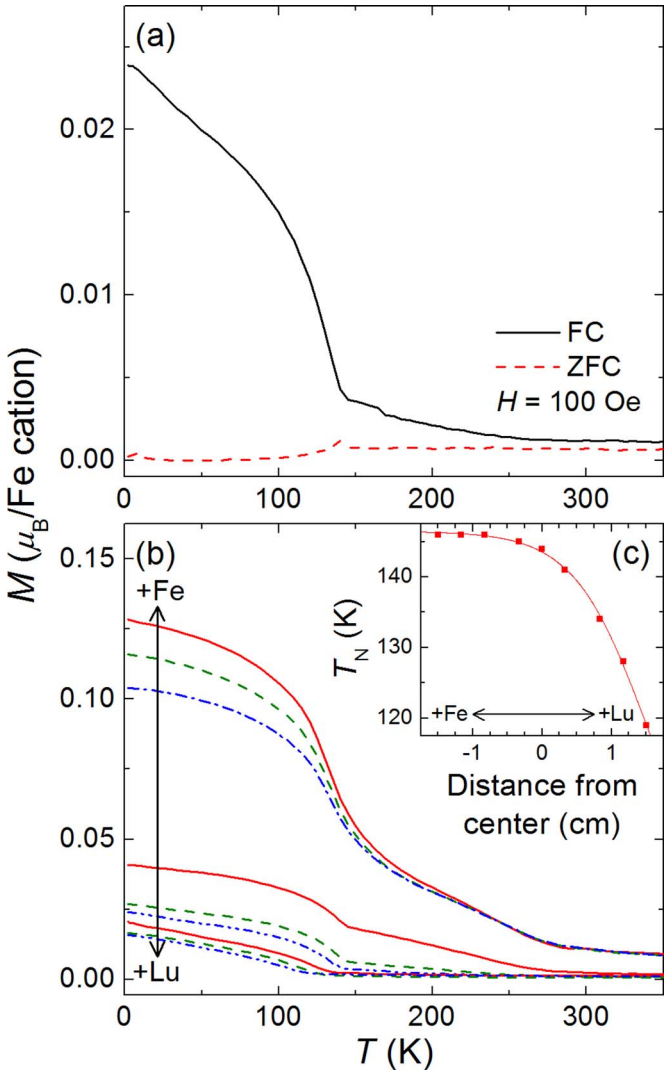

FIG. 4. (a) Out-of-plane *M-T* curves for sample LFO6; measurement was taken at 100 Oe with the sample cooled in either 0 Oe (ZFC) or 1 kOe (FC). (b) Out-of-plane field cooled *M-T* curves for all samples. (c) Variation in T_N of *h*-$LuFeO_3$ with composition; line provided as a guide to the eye.

These phases likely correspond to the $LuFe_2O_4$ intergrowth layers and the Fe_3O_4 precipitates, and have Curie temperatures of ~270 K and greater than 350 K (the temperature limit of the SQUID measurement), respectively. The second phase, however, never completely diminishes, even for the lutetium-rich samples, and is apparent in *M-T* measurements of other *h*-$LuFeO_3$ samples in the literature,[23] giving rise to the possibility that this small signal could be a signature of the high temperature antiferromagnetic order recently reported based on neutron diffraction measurements.[23] Adding lutetium to the films does not add any additional phases, but it results in a reduction of the Néel temperature. Figure 4(c) shows T_N of each sample. As the iron content increases, T_N saturates around 147 K for the iron-rich samples.

It is intriguing that the near-stoichiometric sample, LFO6, while not showing any intergrowths in the STEM and having a smooth surface in the AFM, does show evidence of additional magnetic phases in the *M-T* curves [Fig. 4(a)]. We believe this is due to the samples not being rotated during the composition-spread growth. The STEM images were taken from the middle of LFO6, whereas the magnetometry measured the entire sample. The multiple phases apparent in the magnetization measurements likely arise from the finite composition variation across the 3 mm width of the sample

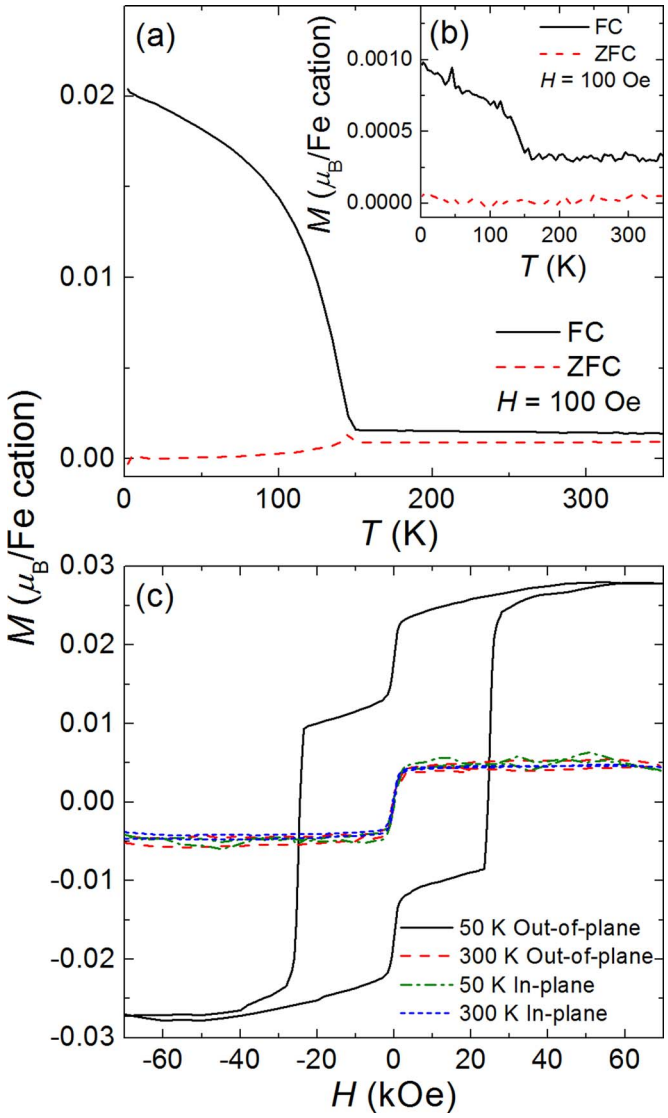

FIG. 5. (a) Out-of-plane *M-T* curves of nominally stoichiometric *h*-$LuFeO_3$ grown by rotating the sample; measurement was taken at 100 Oe with the sample cooled in either 0 Oe (ZFC) or 1 kOe (FC). (b) In-plane *M-T* curves of nominally stoichiometric *h*-$LuFeO_3$. (c) Out-of-plane and in-plane *M-H* loops taken at 50 K and 300 K of nominally stoichiometric *h*-$LuFeO_3$.

in combination with the narrow composition range of single-phase *h*-$LuFeO_3$. We believe that the composition gradient across the composition spread samples results in lutetium rich regions in all the samples except the most iron-rich samples, and a lowering of the Néel temperature in these samples. By rotating the sample during growth, excess iron is no longer needed to eliminate the lutetium deficient regions, and we can now grow a sample that is single phase. In order to obtain a single-phase sample over the entire substrate, an additional film was grown using the elemental fluxes corresponding to the region of LFO6, with the addition of rotating the sample stage to ensure the deposition of homogeneous composition across the film.

Figure 5(a) shows the out-of-plane *M-T* curves of this rotated sample. There is no evidence of the magnetic signature of $LuFe_2O_4$ intergrowths within this sample, although the high temperature magnetic phase is still detectable. It is unclear whether this signal is from iron oxide impurities or a signature of high temperature antiferromagnetic order, and we cannot make any conclusions about this since our SQUID magnetometer is limited in temperature to 350 K. The Néel temperature of

this film is 147 K, which agrees with the saturation of T_N seen in the composition spread samples. Hence, we conclude that the intrinsic Néel temperature of *h*-$LuFeO_3$ is 147 K, which is larger than the values previously reported in the literature of 130 K[23] and 120 K.[22,24] It is possible that previous works attempted to avoid iron-rich impurity phases (e.g., $LuFe_2O_4$ and Fe_3O_4) in their samples by growing under slightly lutetium-rich conditions, resulting in their samples being lutetium rich and having lower Néel temperatures than stoichiometric *h*-$LuFeO_3$.

In-plane *M-T* curves of the nominally stoichiometric sample [Fig. 5(b)] reveal a magnetization that has the same Néel temperature as the out-of-plane measurement, but is reduced by over an order of magnitude (measurements nominally along the [110] and [1$\bar{1}$0] crystallographic axes of *h*-$LuFeO_3$ produced the same results). A slight misalignment of the sample by 2°–3° during the in-plane measurements would result in a small out-of-plane component, which is likely the cause of the measured in-plane magnetizations, confirming that the canted antiferromagnetism in $LuFeO_3$ is aligned along the out-of-plane direction. We thus conclude that the intrinsic in-plane moment of *h*-$LuFeO_3$ is either too small for our technique to measure or nonexistent.

Measurements of the magnetization as a function of magnetic field (*M-H*) allowed for further analysis of the magnetic properties. Figure 5(c) shows out-of-plane and in-plane *M-H* loops, with the diamagnetic background subtracted, measured at 50 and 300 K for the nominally stoichiometric sample. By measuring *M-H* loops at these temperatures, we can distinguish the individual magnetic properties *h*-$LuFeO_3$ from the high temperature magnetic phase. The *h*-$LuFeO_3$ phase has a large coercive field of ∼25 kOe and a saturation magnetic moment of 0.018 μ_B/Fe cation. The in-plane measurements only measure the high temperature magnetic phase, confirming that there is no in-plane magnetization intrinsic to *h*-$LuFeO_3$.

In summary, we determined the intrinsic magnetic properties of *h*-$LuFeO_3$ and have identified the magnetic signatures of different types of defects that can be easily accommodated within this material. While films that contain excess iron and lutetium still appear to be single phase in XRD, both STEM and AFM show that as the nonstoichiometry increases, the excess lutetium and iron cations introduce defects or impurity phases, most notably with excess iron being incorporated as $LuFe_2O_4$ intergrowths and Fe_3O_4 precipitates. In contrast to excess iron, excess lutetium does not add any secondary magnetic phases, but does lead to a decrease in the Néel temperature. This study demonstrates that the magnetic properties of seemingly phase-pure *h*-$LuFeO_3$ samples, as analyzed by XRD, can be sensitive to small changes in composition, and by understanding the signatures of defects in other measurements, such as magnetometry, these defects can be easily identified. The ability to use magnetometry to establish and confirm growth conditions yielding phase-pure *h*-$LuFeO_3$ will enable future studies to investigate the possibility of magneto-electric coupling[25] within this purportedly room-temperature multiferroic.[23]

The authors would like to thank Hena Das and Craig Fennie for helpful discussions. Research supported by the U.S. Department of Energy, Office of Basic Energy Sciences, Division of Materials Sciences and Engineering, under Award No. DE-SC0002334. Julia A. Mundy acknowledges financial support from the Army Research Office in the form of a National Defense Science & Engineering Graduate Fellowship and from the National Science Foundation in the form of a graduate research fellowship. This work was performed in part at the Cornell NanoScale Facility, a member of the National Nanotechnology Infrastructure Network, which is supported by the National Science Foundation (Grant ECCS-0335765) and made use of the electron microscopy facility of the Cornell Center for Materials Research with support from the National Science Foundation (NSF) Materials Research Science and Engineering Centers program (DMR 1120296) and NSF IMR-0417392.

[1] W. Eerenstein, N. D. Mathur, and J. F. Scott, Nature (London) **442**, 759 (2006).
[2] N. A. Spaldin and M. Fiebig, Science **309**, 391 (2005).
[3] M. Bibes and A. Barthelemy, Nat. Mater. **7**, 425 (2008).
[4] N. Hur, S. Park, P. A. Sharma, J. S. Ahn, S. Guha, and S. W. Cheong, Nature (London) **429**, 392 (2004).
[5] S. Dong, J. Zhai, F. Bai, J. F. Li, and D. Viehland, Appl. Phys. Lett. **87**, 062502 (2005).
[6] J. Ryu, S. Priya, K. Uchino, and H. E. Kim, J. Electroceram. **8**, 107 (2002).
[7] S. Shastry, G. Srinivasan, M. I. Bichurin, V. M. Petrov, and A. S. Tatarenko, Phys. Rev. B **70**, 064416 (2004).
[8] A. S. Tatarenko, V. Gheevarughese, and G. Srinivasan, Electron. Lett. **42**, 540 (2006).
[9] N. A. Hill, J. Phys. Chem. B **104**, 6694 (2000).

[10] J. Wang, J. B. Neaton, H. Zheng, V. Nagarajan, S. B. Ogale, B. Liu, D. Viehland, V. Vaithyanathan, D. G. Schlom, U. V. Waghmare, N. A. Spaldin, K. M. Rabe, M. Wuttig, and R. Ramesh, Science **299**, 1719 (2003).
[11] R. Ramesh and N. A. Spaldin, Nat. Mater. **6**, 21 (2007).
[12] H. L. Yakel, E. F. Forrat, E. F. Bertaut, and W. C. Koehler, Acta Crystallogr. **16**, 957 (1963).
[13] K. Lukaszew and J. Karutkal, Ferroelectrics **7**, 81 (1974).
[14] C. J. Fennie and K. M. Rabe, Phys. Rev. B **72**, 100103 (2005).
[15] C. Ederer and C. J. Fennie, J. Phys.: Condens. Matter **20**, 434219 (2008).
[16] C. J. Fennie, Phys. Rev. Lett. **100**, 167203 (2008).
[17] N. Ikeda, H. Ohsumi, K. Ohwada, K. Ishii, T. Inami, K. Kakurai, Y. Murakami, K. Yoshii, S. Mori, Y. Horibe, and H. Kito, Nature (London) **436**, 1136 (2005).
[18] J. de Groot, T. Mueller, R. A. Rosenberg, D. J. Keavney, Z. Islam, J. W. Kim, and M. Angst, Phys. Rev. Lett. **108**, 187601 (2012).
[19] A. Ruff, S. Krohns, F. Schrettle, V. Tsurkan, P. Lunkenheimer, and A. Loidl, Eur. Phys. J. B **85**, 290 (2012).
[20] J. A. Mundy, Q. Y. Mao, C. M. Brooks, D. G. Schlom, and D. A. Muller, Appl. Phys. Lett. **101**, 042907 (2012).
[21] A. A. Bossak, I. E. Graboy, O. Y. Gorbenko, A. R. Kaul, M. S. Kartavtseva, V. L. Svetchnikov, and H. W. Zandbergen, Chem. Mater. **16**, 1751 (2004).
[22] Y. K. Jeong, J. H. Lee, S. J. Ahn, and H. M. Jang, Chem. Mater. **24**, 2426 (2012).
[23] W. Wang, J. Zhao, W. Wang, Z. Gai, N. Balke, M. Chi, H. N. Lee, W. Tian, L. Zhu, X. Cheng, D. J. Keavney, J. Yi, T. Z. Ward, P. C. Snijders, H. M. Christen, W. Wu, J. Shen, and X. Xu, Phys. Rev. Lett. **110**, 237601 (2013).
[24] A. R. Akbashev, A. S. Semisalova, N. S. Perov, and A. R. Kaul, Appl. Phys. Lett. **99**, 122502 (2011).
[25] H. Das, A. L. Wysocki, Y. Geng, W. Wu, and C. J. Fennie, Nat. Comm. **5**, 2998 (2014).
[26] A. A. Belik, S. Iikubo, K. Kodama, N. Igawa, S. Shamoto, S. Niitaka, M. Azuma, Y. Shimakawa, M. Takano, F. Izumi, and E. Takayama-Muromachi, Chem. Mater. **18**, 798 (2006).
[27] M. R. Li, U. Adem, S. R. C. McMitchell, Z. L. Xu, C. I. Thomas, J. E. Warren, D. V. Giap, H. J. Niu, X. M. Wan, R. G. Palgrave, F. Schiffmann, F. Cora, B. Slater, T. L. Burnett, M. G. Cain, A. M. Abakumov, G. van Tendeloo, M. F. Thomas, M. J. Rosseinsky, and J. B. Claridge, J. Am. Chem. Soc. **134**, 3737 (2012).
[28] J. B. Nelson and D. P. Riley, Proc. Phys. Soc. London **57**, 160 (1945).
[29] P. A. van Aken, B. Liebscher, and V. J. Styrsa, Phys. Chem. Min. **25**, 323 (1998).
[30] A. R. Akbashev, V. V. Roddatis, A. L. Vasiliev, S. Lopatin, V. A. Amelichev, and A. R. Kaul, Sci. Rep. **2**, 672 (2012).